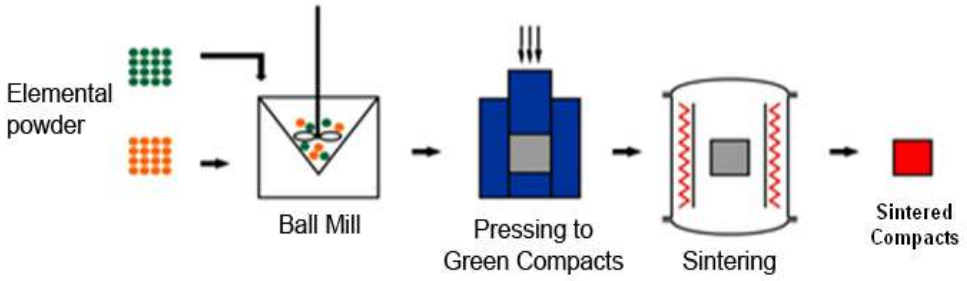

Chapter 4

Synthesis and Characterization Methods

Chapter 4
Synthesis and Characterization Methods

The present chapter focuses on (i) the synthesis and (ii) details of different techniques used for characterizing the metal matrix nanocomposite specimens such as XRD, SEM, density, hardness, wear, deformation and corrosion.

4.1 Synthesis of Specimens

4.1.1 Materials Used

The following powders were used for the purpose of synthesis:

1. Electrolytic Iron metal powder with purity 99.5% and particle size in the range 250-300 mesh (49-58 μm).
2. Aluminium oxide with purity 99.5% and having particle size in the range 70-230 mesh (63-210 μm).
3. Zirconium oxide with purity 99.5% and having particle size in the range 0.8-7 μm.
4. Cobalt oxide (CoO) with purity 99.9 %
5. Cerium oxide (CeO_2) with purity 99.9% and
6. Dextrin powder with purity 99.5% was used as the binder.

   All the chemicals were purchased from Loba Chemie Private Limited Mumbai (INDIA) except for cerium oxide which was purchased from Sigma Aldrich. Iron (Fe) is used as matrix material; aluminium oxide (Al_2O_3) and zirconium oxide (ZrO_2) are used as reinforcement; cobalt oxide (CoO) and cerium oxide (CeO_2) are used as dopants and dextrin ($(C_6H_{10}O_5)_nH_2O$) is used as binder for green compacting.

4.1.2 Weighing and Milling

Depending on the composition appropriate amounts of various chemicals such as iron (Fe), aluminium oxide (Al_2O_3), zirconium oxide (ZrO_2), cobalt oxide (CoO), cerium oxide (CeO_2) and dextrin ($(C_6H_{10}O_5)_nH_2O$) were weighed using an electronic balance having accuracy of 0.0001 gm. Powders were ground and mixed dry using centrifugal ball milling machine (Retsch). Zirconia balls were used as grinding and mixing media. The powder to ball ratio was 1:2 by weight. For example, in Fe- Al_2O_3 nanocomposite system, iron and alumina powder were ball milled for one hour and thereafter 2 wt. % dextrin was added. The whole composition was again ball milled for an hour. In Fe-Al_2O_3-CoO/CeO_2 nanocomposite system, for first 30 min Al_2O_3 and CoO/CeO_2 were ball milled, followed by 30 minute of ball milling after adding iron. Finally 1 hour milling was carried out after the addition of dextrin binder. Table 4.1 4.2 and 4.3 show the compositions of specimens in Fe-Al_2O_3 and Fe-Al_2O_3-CoO/CeO_2 nanocomposite systems. Table 4.4 shows Fe-Al_2O_3-ZrO_2 hybrid metal matrix nanocomposite specimens.

Table 4.1 Compositions of Fe-Al_2O_3 metal matrix nanocomposite specimens in wt%

S. No.	Fe %	Al_2O_3%
1.	95	5
2.	90	10
3.	80	20
4.	70	30

Table 4.2 Compositions of Fe- Al_2O_3-CoO metal matrix nanocomposite specimens in wt%

S. No.	Fe %	Al_2O_3 %	CoO %
1.	90	10	0.5
2.	90	10	1.0
3.	100	00	0.5
4.	100	00	00

Table 4.3 Compositions of Fe-Al_2O_3-CeO_2 metal matrix nanocomposite specimens in wt%

S. No.	Fe %	Al_2O_3 %	CeO_2 %
1.	90	10	0.5
2.	90	10	1.0
3.	100	00	0.5
4.	100	00	00

Table 4.4 Compositions of Fe- Al_2O_3-ZrO_2 hybrid metal matrix nanocomposite specimens in wt%

S. No.	Fe %	Al_2O_3 %	ZrO_2 %
1.	95	2.5	2.5
2.	95	1.5	3.5

4.1.3 Compaction

Initially the compaction of the ball milled powder was done under a load of 5, 6 and 7 tons using high chrome high carbon steel die of diameter 12 mm and a hydraulic press. Initially several binder such as PVA, gum etc were used in varying concentrations and it was observed that 2 wt% dextrin gave the optimum green strength. On the basis of the measured green density of the compacts, it was found that 7 tons load was optimum for satisfactory compaction. Therefore, compaction of all the ball milled powders was done in a die under a load of 7 tons for preparation of all types of specimens.

4.1.4 Sintering

Fe-Al_2O_3 green specimens were sintered in an argon atmosphere in the sintering temperature range of 900-1100°C for 1-3 hours in an indigenously developed atmosphere controlled electrical furnace. Cobalt oxide (CoO) and cerium oxide (CeO_2) doped Fe-Al_2O_3 green specimens were sintered at 1100°C for 1 hour. Fe-

Al_2O_3-ZrO_2 hybrid nanocomposite specimens were sintered in the range of 900-1100°C for 1-3 hours in an argon atmosphere controlled furnace. Binder removal from the specimens was done by heating in a furnace at 500°C and holding it for 1h before taking them to the required sintering temperature. The heating and cooling of the furnace was done at a rate of 5°C/min employing PID temperature controller.

4.2 Characterization Techniques

The structural characterization of the sintered specimens was carried out using X-ray diffraction (XRD), scanning electron microscopy (SEM). Mechanical characterizations were done by measuring hardness, wear and deformation. Electrochemical characterization was carried out by using the Tafel polarization corrosion measurement technique.

4.2.1 X-ray Diffraction (XRD)

X-ray diffraction is a non-destructive technique widely used for the characterization of crystallographic structure of the material. The method has been extensively used for phase identification, quantitative analysis and determination of structure imperfections.

The principle of XRD technique is based on scattering of X-rays by a crystal consisting of well-defined array of atoms, ions or molecules. Since the crystal lattice consists of parallel arrays of atoms equivalent to the parallel lines of the diffraction grating, the inter-planar spacing could be successfully determined from the separation of bright fringes of the diffraction pattern. These inter planar spacings are of the same magnitude as the wavelength of X-rays (0.5Å to 2.0Å) and hence crystal planes act as diffraction gratings. Interaction of X-rays reflected by a set of parallel planes satisfying Bragg's condition lead to constructive interference only at a particular angle [Cullity (1956); Marchesini (2003)]. The Bragg condition for the occurrence of such diffraction can be written as:

$$n\lambda = 2dSin\theta \quad (4.1)$$

where λ is wavelength of X-rays, θ is the glancing angle (called as Bragg's angle), d is the inter-planar separations and n is the order of diffraction. n is taken as 1. The theta-theta goniometer has been used in the reflection geometry. A thick layer of powdered sample spread over a Perspex plate coated with a thin layer of high vacuum grease was used for recording the X-ray diffraction patterns. The XRD data provide the variation of intensity/counts per second (cps), (recorded by the detector, scintillation counter) as a function of 2θ where θ is the incidence angle [Stanjek and Hausler (2004)].

The Phase determination of all the samples except CeO_2 doped specimens was done by powder X-ray diffraction (XRD) using Rigaku Desktop Miniflex II X-Ray diffractometer employing Cu-Kα radiation and Ni-filter. XRD pattern of cerium oxide doped specimen was carried out using Proto AXRD Bench top Powder diffractometer with Cu X-Ray tube. Diffraction peaks present in the specimen was matched with the XRD – JCPDS files of different constitutent compounds which might have been formed during sintering. The particle size (D) was found out from the Scherrer formula given by equation:

$$D=0.9\lambda/\beta\cos\theta \quad (4.2)$$

where λ is the wavelength of X-ray, β is the full width at half maxima and θ is the angle of diffraction.

4.2.2 Scanning Electron Microscopy (SEM)

Scanning electron microscope is an instrument which is used to observe the morphology of a sample at higher magnification, resolution and depth of focus compared with the optical microscope. A well-focused mono energetic (approx. 5keV-25keV) beam is incident on a solid surface giving different scattering processes on the surface. In case of SEM, secondary electrons (SE) and back scattered electrons

(BSE) are particularly used to see the morphology on the sample surface. BSE or SE are collected and converted into current signals. The signal is amplified and utilized to control the brightness of the spot on the cathode ray tube/screen of monitor [Stanley et al. (1993); Kazemian et al. (2007)].

Secondary electron mode (SE) is created by collision between the high-energy electrons beam and the electrons which surround the atoms in the sample. Such collisions knock out the lower energy electrons out of their orbits. Strength of secondary electrons depend on the beam size, beam current, angle of incidence, the topography and the atomic number of the sample [Sakai et al. (1999)].

Back scattered mode is created by collision between the primary beam electrons and the nuclei of the target atoms. These collisions result in the primary electrons bouncing off the larger, more massive nuclei. The escape depth is comparatively large because of the large energy of the back scattered electrons. The method gives contrast even in the flat samples due to compositional distribution. BSE images can give important information about the spatial relationships of adjacent phases plus about the zoning and inclusions within the phases. BSE intensity is, to a first approximation, a function of the chemical composition. The brighter an area, the greater is its mean atomic number relative to adjacent areas [Wight and Konicek (2012)].

Energy-dispersive X-ray spectroscopy (EDS, EDX, or XEDS), sometimes called energy dispersive X-ray analysis (EDXA or EDAX) or energy dispersive X-ray microanalysis (EDXMA), is an analytical technique used for the elemental analysis or chemical characterization of a sample. It relies on interaction of electron beam with specimens for excitation of characteristic X-rays from their constituent elements. Its characterization capabilities are due in large part to the fundamental principle that each element has a unique atomic structure allowing unique set of X-rays emission spectrum. To stimulate the emission of characteristic X-rays from a specimen, a high-energy beam of charged particles such as electrons or protons, or a beam of X-rays is focused on the sample being studied. At rest, an atom within the sample contains

ground state (or unexcited) electrons in discrete energy levels or electron shells bound to the nucleus. The incident beam may excite an electron in an inner shell ejecting it from the shell while creating an electron hole where the electron originally was. An electron from an outer, higher-energy shell then fills the hole and the difference in energy between the higher-energy shell and the lower energy shell may be released in the form of an X-ray. The number and energy of the X-rays emitted from a specimen can be measured by an energy-dispersive spectrometer. As the energy of the X-rays are characteristic of the difference in the energy between the two shells and of the atomic structure of the element from which they were emitted, this allows the elemental composition of the specimen to be measured.

Special preparation must be done for the sample because the SEM utilizes vacuum conditions and uses electrons to form an image. All water must be removed from the samples because water would evaporate in vacuum. Since all the metals are conducting in nature, they require no preparation before being used. But non-metals need to be made conductive and thus non-metallic samples are covered with a thin layer of a conductive material. This is done by using a device called a sputter coater. The sputter coater uses argon gas and an electric field. The sample is placed in a small evacuated chamber. Electric field causes an electron to be removed from the argon, making the argon atoms positively charged and the argon ions get attracted towards negatively charged gold foil. As a result the argon ions knock off the gold atoms from the surface of the gold foil. These gold atoms fall and get settled onto the surface of the sample to be coated producing a thin gold coating on the sample.

In the present investigations, before recording the SEM of the sintered specimens they were cut having a height of 2.5 mm and polished using various grades of emery papers (1/0, 2/0, 3/0 and 4/0). After polishing the specimens using emery papers, the specimens were polished using alumina gel followed by drying the specimen in an oven overnight. Finally the specimen surface was polished using the hifin fluid and diamond paste of size 12 μm, 6 μm and 0.5 μm respectively. After polishing the specimen was etched using HCl solution for 20 seconds.

The microstructure of the deformed specimens was studied by cutting the specimens in transverse directions. Thereafter, the specimen was polished using various grades of emery paper (1/0, 2/0, 3/0 and 4/0). After polishing the specimens with emery papers the specimens were polished using alumina gel followed by drying the specimen in an oven overnight. Finally the specimen surface was polished using the hifin fluid and diamond paste of size 12 µm, 6 µm and 0.5 µm respectively. After polishing, the specimen was etched using HCl solution for 20 seconds. EDX of the representative nanocomposite specimen was carried out in order to confirm the composition of the phases present.

Microstructure of the worn surfaces of the specimens was also observed by using SEM. The weared pin specimens were cut with an appropriate height of 2.5 mm for easy mounting. Before mounting, the specimens were cleaned with the help of tissue paper moistened with acetone to remove any debris, oil or grease.

Similarly, microstructures along with EDX of the corroded specimens were also recorded using SEM after cleaning the surface of the specimen with the help of acetone and tissue paper and drying it in hot air oven for 24 hour respectively.

Microstructure was studied using Inspect S-50, FP 2017/12 scanning electron microscope; FEI QUANTA 200 FEG field emission scanning electron microscope and SUPRA 40, Zeiss Field Emission Scanning Electron Microscope (FESEM) and Hitachi S-4800 field emission scanning electron microscope.

4.2.3 Density

Measurement of green density measurement was carried out in the following manner. Let D_g be the density of the specimen in the green state. Let, m_g= mass, r_g= radius, h_g= height and V_g= Volume of the specimen after compaction in the green state, Then,

$$D_g = m_g / V_g = m_g / (\pi r_g^2 h_g) \quad (4.3)$$

The density was calculated after sintering in the following manner:
Let, D_s be the sintered density, m_s= mass, r_s= radius, h_s= height and V_s= Volume of the specimen after sintering, Then,

$$D_s = m_s / V_s = m_s / (\pi r_s^2 h_s) \quad (4.4)$$

For the deformed specimens density was measured using the Archimedes principle.

Let, wt. of the dry sample = W_d ,
Wt. of the sample suspended in water after boiling it for 2hours = W_s
and Wt. of water absorbed in the sample = W_a.

Then,

$$\text{Apparent Density} = W_d / (W_a - W_s) \quad (4.5)$$

$$\% \text{ Open Porosity} = (W_a - W_d) / (W_a - W_s) \times 100 \quad (4.6)$$

and $$\text{True Density} = W_d / (W_d - W_s) \times d_w \quad (4.7)$$

where d_w is the density of water.

4.2.4 Hardness

Hardness is a surface property of a material by virtue of which it resists indentation/penetration and abrasion. Alternatively, hardness is a measure of resistance shown by the material to various kinds of permanent shape changes when a force is applied. The Metals Handbook defines hardness as "Resistance of a metal to plastic deformation, usually by indentation. However, the term may also refer to stiffness or temper or resistance to scratching, abrasion, or cutting. It is the property of a metal which gives it the ability to resist being permanently deformed (bent,

broken, or have its shape changed) when a load is applied [Cheng and Cheng (2000)]. Greater the hardness of the metal, greater is the resistance it has to deformation. There are three types of Hardness depending on measuring method; Scratch hardness, Indentation hardness and Rebound hardness.

(a) Scratch Hardness:

Scratch hardness is the measure of how resistant a sample is to fracture or plastic (permanent) deformation due to friction from a sharp object. The principle is that an object made of a hard material will scratch an object made of a softer material. The most common test is Mohs scale which is used in mineralogy. One tool to make this measurement is the sclerometer.

(b) Indentation Hardness:

Indentation hardness measures the resistance of a sample to permanent plastic deformation due to a constant compression load from a sharp object. These are primarily used in engineering and metallurgy fields [Zhang et al. (2011)]. Common indentation hardness scales are Rockwell, Vickers, and Brinell.

(c) Rebound hardness:

Rebound hardness also known as *dynamic hardness* measures the height of the "bounce" of a diamond-tipped hammer dropped from a fixed height onto a material. Two scales which measure rebound hardness are the Leeb Rebound hardness and Bennett hardness scale.

Hardness testing methods:

Various methods used worldwide for the measurement of the hardness are as follows:-

(i) Shore Hardness Test

The shore scleroscope measures hardness in terms of the elasticity of the material. A diamond-tipped hammer in a graduated glass tube is allowed to fall from a known height on the specimen to be tested and the hardness number depends on the height to which the hammer rebounds; the harder the material, the higher the rebound. Shore hardness is a measure of the resistance of material to indentation by a 3 spring-loaded indenter. The higher the number, the greater is the resistance.

(ii) Barcol's hardness test

The Barcol hardness test characterizes the indentation hardness of materials by the depth of penetration of an indentor loaded on the material sample as compared to the penetration in a reference material. The method is most often used for composite materials such as reinforced thermosetting resins or to determine how much a resin or plastic has cured. The test complements the measurement of glass transition temperature as an indirect measure of the degree of cure of a composite. It is inexpensive and quick and provides information on the cure throughout a part.

(iii) Rockwell Hardness Test

Rockwell Hardness test is a hardness measurement based on the net increase in the depth of impression as a load is applied. Hardness numbers have no units and are commonly given in the A, B, C, H, K, L, M and R scales. The higher the number in each of the scales, harder is the material. In the Rockwell method of hardness testing, the depth of penetration of an indenter under certain arbitrary test conditions is determined. The indenter may either be a steel ball of some specified diameter or a spherical diamond-tipped cone of 120° angle and 0.2 mm tip radius called Brale. This test measures the difference in the depth caused by two different forces, using a dial gauge.

Table 4.5 Rockwell Hardness Scales

Scale	Indenter	Minor Load (F_0) kgf	Major Load (F_1) kgf	Total Load (F) kgf	Value of E
A	Diamond Cone	10	50	60	100
B	1/16” steel ball	10	90	100	130
C	Diamond Cone	10	140	150	100
D	Diamond Cone	10	90	100	100
E	1/8” steel ball	10	90	100	130
F	1/16” steel ball	10	50	60	130
G	1/16” steel ball	10	140	150	130
H	1/8” steel ball	10	50	60	130
K	1/8” steel ball	10	140	150	130
L	1/4” steel ball	10	50	60	130
M	1/4” steel ball	10	90	100	130
P	1/4” steel ball	10	140	150	130
R	1/2” steel ball	10	50	60	130
S	1/2” steel ball	10	90	100	130
V	1/2” steel ball	10	140	150	130

Using standard hardness conversion tables, the Rockwell hardness value is determined for the load applied, the diameter of the indenter and the indentation depth [Mishra et al. (2014)]. Table 4.5 shows the rockwell hardness scales. The test on Rockwell hardness tester is done in the following manner:

- The Rockwell hardness test method consists of indenting the test material with a diamond cone or hardened steel ball indenter.
- The indenter is forced into the test material under a preliminary minor load usually 10 kgf.
- When the equilibrium has been attained, an indicating device, which follows the movements of the indenter and so responds to changes in the depth of penetration of the indenter is set to a datum position.
- While the preliminary minor load is still applied, an additional major load is applied with resulting increase in penetration. Again after equilibrium, the

additional major load is removed but the preliminary minor load is still maintained.

- Removal of the additional major load allows a partial recovery. This reduces the depth of penetration. Thus, the hardness number is read directly on the scale of the gauge.

(iv) Brinell Hardness Test

Brinell hardness is determined by forcing a hard steel or carbide sphere of a specified diameter under a specified load on the surface of a material and measuring the diameter of the indentation left after the test. The Brinell hardness number (BHN), or simply the Brinell number is obtained by dividing the load used in kilograms by the actual surface area of the indentation in square millimeters. The result is a pressure measurement but the units are rarely stated. The BHN is calculated according to the following formula:

$$BHN = \frac{2F}{\pi D.(D-\sqrt{D^2-D_i^2})} \quad (4.8)$$

Where

BHN = Brinell hardness number
F = the applied load (measured in kg)
D = the diameter of the spherical indenter (measured in mm)
D_i = diameter of the resulting indenter impression (measured in mm)

(v) Vickers Hardness Test

It is the standard method for measuring the hardness of metals, particularly those with extremely hard surfaces. Vickers hardness is a measure of the hardness of a material calculated from the size of an impression produced under a load by a pyramid-shaped diamond indenter. The indenter employed in the Vickers test is a square-based pyramid whose opposite sides meet at the apex at an angle of 136º. In this test the

surface is subjected to a standard pressure for a standard length of time by means indenter. The diagonal of the resulting indention is measured under a microscope and the Vickers Hardness value read from a conversion table [Wan and Gong (2003)].
The Vickers number (HV) is calculated using the following formula:

$$HV = 1.854(F/D^2) \tag{4.9}$$

with F being the applied load (measured in kilograms-force) and D^2 the area of the indentation (measured in square millimetres). The applied load is usually specified when HV is cited.

(vi) Knoop Hardness Test

The relative microhardness of a material is determined by the Knoop indentation test. In this test, a pyramid-shaped diamond indenter with apical angles of 130° for the short edge and 172° for long edge (called a Knoop indenter) is pressed against a material making a thombohedral impression with one diagonal seven times longer than the other. The hardness of the material is determined by the depth to which the Knoop indenter penetrates. The diamond indenter employed in the Knoop test is in the shape of an elongated four-sided pyramid with the angle between the two of the opposite faces being approximately 170º and the angle between the other two being 130º. The final Knoop hardness (HK) is derived from the following formula:

$$HK = \frac{\text{load(kgf)}}{\text{impression area(mm}^2\text{)}} = \frac{P}{C_p L^2} \tag{4.10}$$

Where

P = load applied (measured in kilograms-force)
C_p = correction factor related to the shape of the indenter, ideally 0.070279
L = length of indentation along its long axis (measured in square millimetres)

(vii) Microhardness test

The term microhardness test usually refers to static indentations made with loads not exceeding 1 kg. The indenter is either the Vickers diamond pyramid or the Knoop elongated diamond pyramid. The procedure for testing is very similar to that of the standard Vickers hardness test, except that it is done on a microscopic scale with higher precision instruments. The surface being tested generally requires a metallographic finish; the smaller the load used, the higher the surface finish required. Precision microscopes are used to measure the indentations; these usually have a magnification of around 500X and measure with an accuracy of $\pm$0.5 micrometres. Also with the same observer differences of $\pm$0.2 micrometres can usually be resolved. It should, however, be added that considerable care and experience are necessary to obtain this accuracy.

In the present case the hardness of all the sintered specimens was measured on a Rockwell Hardness tester with 1/8 inch H scale steel ball indenter and a load of 60 kg. Reading of the H type indenter was read on the red scale present on the dial gauge of the instrument. Initially a minor load (10 kg) is applied on the specimen and after that major load is applied on the specimen by turning the lever to the loading position.

4.2.5 Wear

Wear is erosion or sideways displacement of material from its "derivative" and original position on a solid surface performed by the action of one on another surface. Wear is related to interactions between the surfaces and more specifically the removal and deformation of material from a surface as a result of mechanical action of the opposite surface. The need for relative motion between two surfaces and initial mechanical contact between asperities is an important distinction between mechanical wear compared to other processes with similar outcome [Xie (1999)].

The definition of wear may include loss of dimension from plastic deformation if it is originated at the interface between two sliding surfaces. However, plastic deformation such as yield stress is excluded from the wear definition if it doesn't incorporate a relative sliding motion and contact against another surface despite the possibility for material removal because it then lacks the relative sliding action of another surface. Impact wear is in reality a short sliding motion where two solid bodies interact at an exceptional short time interval. Previously due to the fast execution, the contact found in impact wear was referred to as an impulse contact by the nomenclature. Impulse can be described as a mathematical model of a synthesized average on the energy transport between two travelling solids in opposite converging contact [Priest and Taylor (2000)].

(1) Stages of Wear

Under normal mechanical and practical procedures, the wear-rate normally changes through three different stages [Pogosian (1998)]:

- Primary stage or early run-in period, where surfaces adapt to each other and the wear-rate might vary between high and low.
- Secondary stage or mid-age process, where a steady rate of ageing is in motion. Most of the components operational life is comprised in this stage.
- Tertiary stage or old-age period, where the components are subjected to rapid failure due to a high rate of aging.

The secondary stage is shortened with increasing severity of environmental conditions such as higher temperatures, strain rates, stress and sliding velocities etc. It is quite notable that the wear rate is strongly influenced by the operating conditions. Specifically, normal loads and sliding speeds play a vital role in determining the wear rate. In addition, tribo-chemical reaction is also important in order to understand the wear behavior. Different oxide layers are developed during the sliding motion. The layers originate from the complex interaction among the surface, lubricants and

environmental molecules. Demonstrating wear rate under different loading condition is used for operation. This graph also represents dominating wear modes under different loading conditions.

In explicit wear tests simulating industrial conditions between metallic surfaces, there are no clear chronological distinction between different wear-stages due to big overlaps and symbiotic relations between various friction mechanisms. Surface engineering and treatments are used to minimize wear to extend the components working life.

(2) Types of Wear

The study of the processes of wear is a part of the discipline of tribology. The complex nature of wear has delayed its investigations and resulted in isolated studies towards specific wear mechanisms or processes [Taylor (1998)]. Some commonly referred to wear mechanisms (or processes) include:

(a) Adhesive wear

Adhesive wear can be found between surfaces during frictional contact and generally refers to unwanted displacement and attachment of wear debris and material compounds from one surface to another. Two separate mechanisms operate between the surfaces. Generally, adhesive wear occurs when two bodies slide over or are pressed against each other which promote material transfer. This can be described as plastic deformation of very small fragments within the surface layers. The asperities or microscopic high points or surface roughness found on each surface define the severity on how fragments of oxides are pulled off and adds to the other surface, partly due to strong adhesive forces between atoms but also due to accumulation of energy in the plastic zone between the asperities during relative motion.

(b) Abrasive wear

Abrasive wear occurs when a hard rough surface slides across a softer surface. ASTM International (formerly American Society for Testing and Materials) defines it as the loss of material due to hard particles or hard protuberances which are forced against and move along a solid surface.

Abrasive wear is commonly classified according to the type of contact and the contact environment. The type of contact determines the mode of abrasive wear. The two modes of abrasive wear are known as two-body and three-body abrasive wear. Two-body wear occurs when the grits or hard particles remove material from the opposite surface. The common analogy is that of material being removed or displaced by a cutting or plowing operation. Three-body wear occurs when the particles are not constrained and are free to roll and slide down a surface. The contact environment determines whether the wear is classified as open or closed. An open contact environment occurs when the surfaces are sufficiently displaced to be independent of one another.

(c) Surface fatigue

Surface fatigue is a process by which the surface of a material is weakened by cyclic loading. This is one type of general material fatigue. Fatigue wear is produced when the wear particles are detached by cyclic crack growth of micro cracks on the surface. These micro cracks are either superficial cracks or subsurface cracks.

(d) Fretting wear

Fretting wear is the repeated cyclical rubbing between the two surfaces over a period of time which will remove material from one or both surfaces in contact. It occurs typically in bearings, although most bearings have their surfaces hardened to resist the problem. Another problem occur known as fretting fatigue when cracks in either

surface are created. It is the more serious of the two phenomena because it can lead to catastrophic failure of the bearing. An associated problem occurs when the small particles removed by wear are oxidized in air. The oxides are usually harder than the underlying metal so wear accelerates as the harder particles abrade the metal surfaces further. Fretting corrosion acts in the same way especially when water is present. Unprotected bearings on large structures like bridges can suffer serious degradation in behaviour especially when the salt is used during winter to deice the highways carried by the bridges.

(e) Erosive wear

Erosive wear can be described as an extremely short sliding motion and is executed within a short time interval. Erosive wear is caused by the impact of particles of solid or liquid against the surface of an object. The impacting particles gradually remove material from the surface through repeated deformation and cutting action. It is a widely encountered mechanism in industry. A common example is the erosive wear associated with the movement of slurries through piping and pumping equipment.

The rate of erosive wear is dependent upon a number of factors. The material characteristics of the particles such as their shape, hardness, impact velocity and impingement angle are primary factors along with the properties of the surface being eroded. The impingement angle is one of the most important factors and is widely recognized in literature. For ductile materials, the maximum wear rate is found when the impingement angle is approximately 30° whilst for non ductile materials, the maximum wear rate occurs when the impingement angle is normal to the surface.

(3) Determination of Wear using Pin on Disc Wear and Friction Testing Machine

Fig. 4.1 shows the schematic layout of pin on disc wear and friction testing machine The system consists of a motor driven spindle and chuck for holding the revolving disc, a lever-arm device to hold the pin and attachments to allow the pin specimen to

be forced against the revolving disc specimen with a controlled load. A variable speed motor, capable of maintaining constant speed (±1% of rated full load motor speed) under load is required. The motor should be mounted in such a manner that its vibration does not affect the test. Rotating speeds are typically in the range 100 rpm to 3000 rpm. Pin specimen is mounted on stationary specimen holder, which is attached to a lever arm that has a pivot. Adding weights, as one option of loading, produces a test force proportional to the mass of the weights applied. Ideally, the pivot of the arm should be located in the plane of the wearing contact to avoid extraneous loading forces due to the sliding friction. The pin holder and arm must be of substantial construction to reduce vibrational motion during the test.

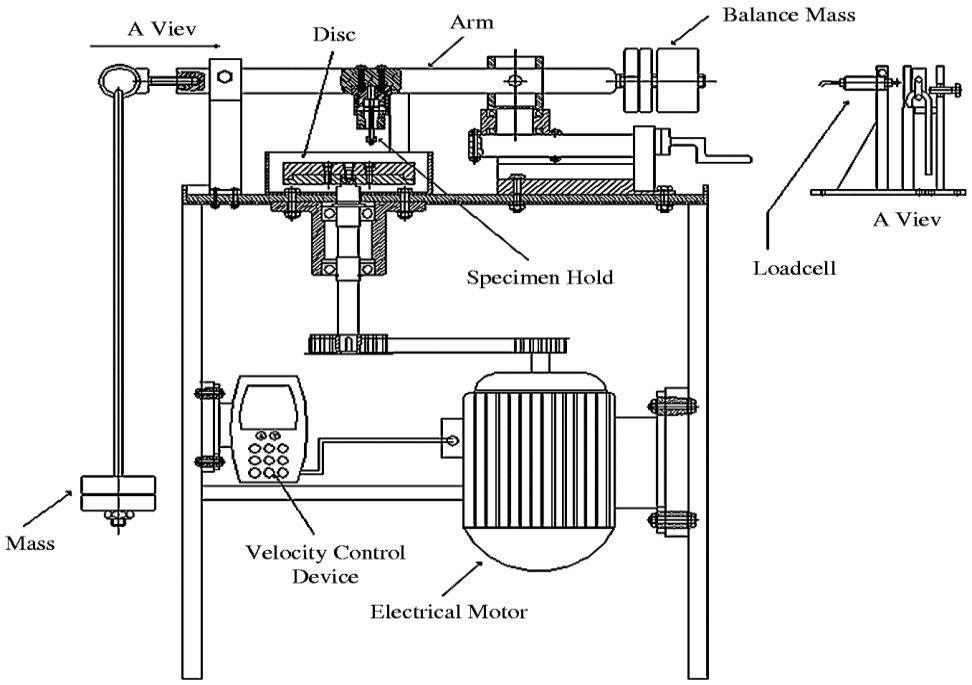

Fig. 4.1 Schematic Layout of Pin on Disc Wear and Friction Testing Machine
[Source: www.emeraldinsight.com]

Another type of system loads a pin revolving about the disc centered against a stationary disc. In any case, the wear track on the disc is a circle involving multiple wear passes on the same track. The machine is equipped with a revolution counter or its equivalent that will record the number of disc revolutions and preferably have the ability to shut off the machine after a pre-selected number of revolutions. The system

has a friction force measuring system, for example, a load cell that allows the coefficient of friction to be determined [Holmberg (2001)]. Wear is determined by the measurement of material volume loss (mm^3) per unit relative distance travelled (km). There is a wear measuring system which is a device to obtain linear measures of wear having a sensitivity of 2.5 μm or better. Linear wear loss is also measured by the measurement of mass loss of the test specimen using a balance with a sensitivity of 0.1 mg or better.

Following steps are adopted for carrying out the wear measurement:

1) For the pin-on-disc wear test, two specimens are required. One, a pin with a round tip, is positioned perpendicular to the other, usually a flat circular disc. A ball, rigidly held, is often used as the pin specimen. The test machine causes either the disc specimen or the pin specimen to revolve about the disc center. In either case, the sliding path is a circle on the disc surface. The plane of the disc may be oriented either horizontally or vertically.

2) The pin specimen is pressed against the disc at a specified load usually by means of an arm or lever and attached weights. Other loading methods have also been used, such as hydraulic or pneumatic.

3) Wear results are reported as volume loss in cubic millimeters for the pin and the disc separately. When two different materials are tested, it is recommended that each material be tested in both the pin and disc positions.

4) The amount of wear is determined by measuring appropriate linear dimensions of both the specimens before and after the test or by weighing both the specimens before and after the test. If linear measures of wear are used, the length change or shape change of the pin and the depth or shape change of the disc wear track (in millimeters) are determined by any suitable metrological technique such as electronic distance gaging or stylus profiling. Linear measures of wear are converted to wear

volume (in cubic millimeters) by using appropriate geometric relations. Linear measures of wear are used frequently in practice since mass loss is often too small to measure precisely. If loss of mass is measured, the mass loss value is converted to volume loss (in cubic millimeters) using an appropriate value for the specimen density.

5) Wear results are usually obtained by conducting a test for a selected sliding distance and for selected values of load and speed. Wear results may in some cases be reported as plots of wear volume versus sliding distance using different specimens for different distances. Such plots may display non-linear relationships between wear volume and distance over certain portions of the total sliding distance and linear relationships over other portions. Causes for such differing relationships include initial "break-in" processes, transitions between regions of different dominant wear mechanisms, etc. The extent of such non-linear periods depends on the details of the test system, materials, and test conditions.

6) It is not recommended that continuous wear depth data obtained from position-sensing gauges be used because of the complicated effects of wear debris and transfer films present in the contact gap and interference from thermal expansion or contraction.

In the present case, measurement of dry sliding wear was carried out using pin on disc wear and friction testing machine (Magnum Engineers, Bangalore, India) using cylindrical pin specimens of 12 mm diameter. Prior to the test, the disc (hardened steel disc with a hardness of HRC 60) was ground using an alumina wheel and then polished using various grades of emery papers to remove the erosion marks. Initially, the composite pin was loaded against a rotating disc and made to run under a load of 2.0 Kg for 2h so that wear occurs on the total surface of the pins during measurements. Sliding velocity is kept as 4 m/sec and the test is performed for 1h. Wear characteristics were studied under a load of 0.5, 1.0 and 2.0 Kg respectively. Wear debris were removed from the surface of the plate intermittently using tissue

paper moistened with acetone. Two readings were taken for each load. The weight loss of the composite pin was measured at intervals of 1h in an analytical balance having 0.0001g precision. The wear volume was then calculated from the values of weight loss.

4.2.6 Deformation

Deformation is the capacity of the material to withstand loads tending to change its shape and/ or size. In materials science, deformation refers to any changes in the shape or size of an object due to-

(a) An applied force (the deformation energy in this case is transferred through work) or

(b) A change in temperature (the deformation energy in this case is transferred through heat).

The first case can be a result of tensile (pulling) forces, compressive (pushing) forces, shear, bending or torsion (twisting).

In the second case, the most significant factor, which is determined by the temperature, is the mobility of the structural defects such as grain boundaries, point vacancies, line and screw dislocations, stacking faults and twins in both crystalline and non-crystalline solids. The movement or displacement of such mobile defects is thermally activated and thus limited by the rate of atomic diffusion.
On an atomic level, the molecules or atoms are forced together when they are in compression. Since atoms in solids always try to find an equilibrium position and distance between other atoms forces arise throughout the entire material which oppose the applied compressive force [Rabiei et al. (2008)].

Deformation testing is a useful procedure for measuring the plastic flow behavior and ductile fracture limits of a material. Moreover, a compression test determines

behavior of materials under crushing loads. Deformation behavior is measured on a universal testing machine. During deformation test, the specimen is deformed at an increasing load until the specimen bulges to its maximum level [Rees (1998)]. Compressive stress and strain are calculated and plotted as a stress-strain diagram which is used to determine elastic limit, proportional limit, yield point, yield strength and for some materials compressive strength [Davis et al (1998)].

In the present case **deformation** of the specimen was carried using a 12 Ton Universal Testing Machine under dry, solid lubricating (Graphite Powder) and liquid lubricating (Oil) conditions. The microstructure of the deformed specimens was carried out by cutting the specimens in transverse directions. The bulge profiles were measured considering top, middle and bottom point of the deformed specimens and the same was drawn using AUTOCAD 2008.

After the deformation of the nanocomposite specimens, theoretical density was calculated using following expressions [Jha and Kumar (1988)]:

Theoretical density d_{th} of the sintered porous composite is given by

$$d_{th}=(\rho_{Inst})x(d_f) \tag{4.11}$$

Where d_f: Density of the deformed solid composite found experimentally and Instantaneous relative density (ρ_{Inst}) of the sintered porous composite during compression under pressure (p) is given as

$$\rho_{Inst} = 1\text{-}\exp\left(\frac{-3p}{2\sigma_c}\right) \tag{4.12}$$

Where σ_c: Yield strength of the sintered porous composite and during compression may be taken as

$$\sigma_c=\frac{\rho_i^k \sigma_0}{1-2\eta} \tag{4.13}$$

Where ρ_i: Initial relative density of the sintered porous composite; σ_o: Yield strength of the solid composite taken as 97.3 MPa [18]; k: constant equal 2 in the yield criteria and η: is a function of relative density ρ_i only.

Calculated theoretical densities of the specimens have been further discussed in the results and discussions part of the present thesis.

4.2.7 Corrosion

Corrosion is the gradual destruction of materials (usually metals) by chemical reaction with its environment. In the most common use of the word, this means electrochemical oxidation of metals in reaction with an oxidant such as oxygen. Rusting, the formation of iron oxides is a well-known example of electrochemical corrosion. This type of damage typically produces oxide(s) or salt(s) of the original metal. Corrosion can also occur in materials other than metals such as ceramics or polymers, although in this context, the term degradation is more common. Corrosion degrades the useful properties of materials and structures including strength, appearance and permeability to liquids and gases [Hihara and Latanision (1994)].

Many structural alloys corrode merely from exposure to moisture in air but the process can be strongly affected by exposure to certain substances. Corrosion can be concentrated locally to form a pit or crack or it can extend across a wide area more or less uniformly corroding the surface. Because corrosion is a diffusion-controlled process, it occurs on exposed surfaces. As a result, methods to reduce the activity of the exposed surface such as passivation and chromate conversion can increase a material's corrosion resistance. However, some corrosion mechanisms are less visible and less predictable.

Mechanism of Corrosion

When a metal specimen or a metal based nanocomposite specimen is immersed in a corrosive medium, both reduction and oxidation processes occur on its surface. Typically, the specimen oxidizes (corrodes) and the medium (solvent) is reduced. In acidic media, hydrogen ions are reduced. The specimen must function as both anode and cathode and both anodic and cathodic currents occur on the specimen surface. All corrosion processes which occur are usually a result of anodic currents [Shreepathi et al. (2010); Tiwari et al. (2007)].

When a specimen is in contact with a corrosive liquid and the specimen is not connected to any instrument – as it would be "in service" – the specimen assumes a potential (relative to a reference electrode) termed the corrosion potential, E_{corr}. A specimen at E_{corr} has both anodic and cathodic currents present on its surface. However, these currents are exactly equal in magnitude so there is no net current to be measured. The specimen is at equilibrium with the environment (even though it may be visibly corroding!). E_{corr} can be defined as the potential at which the rate of oxidation is exactly equal to the rate of reduction.

It is important to stress that when a specimen is at E_{corr} both polarities of current are present. If the specimen is polarized slightly more positive than E_{corr}, then the anodic current predominates at the expense of the cathodic current. As the specimen potential is driven further positive, the cathodic current component becomes negligible with respect to the anodic component. A mathematical relationship exists which relates anodic and cathodic currents to the magnitude of the polarization. Obviously, if the specimen is polarized in the negative direction, the cathodic current predominates and the anodic component becomes negligible.

Types of Corrosion

There are basically five types of corrosion namely:

1) Galvanic Corrosion

Galvanic corrosion occurs when two different metals have physical or electrical contact with each other and are immersed in a common electrolyte or when the same metal is exposed to electrolyte with different concentrations. In a galvanic couple, the more active metal (the anode) corrodes at an accelerated rate and the more noble metal (the cathode) corrodes at a retarded rate. When immersed separately, each metal corrodes at its own rate. What type of metal(s) to use is readily determined by following the galvanic series. For example, zinc is often used as a sacrificial anode for steel structures. Galvanic corrosion is of major interest to the marine industry and also anywhere water (containing salts) contacts pipes or metal structures. Factors such as relative size of anode, types of metal, and operating conditions (temperature, humidity, salinity, etc.) affect galvanic corrosion. The surface area ratio of the anode and cathode directly affects the corrosion rates of the materials. Galvanic corrosion is often prevented by the use of sacrificial anodes [Mansfeld (1971)].

2) Pitting Corrosion

Certain conditions, such as low concentration of oxygen or high concentration of species such as chloride which complete as anions can interfere with a given alloy's ability to re-form a passivating film. In the worst case, almost all of the surface will remain protected but tiny local fluctuations will degrade the oxide film at a few critical points. Corrosion at these points will be greatly amplified and can cause corrosion pits of several types depending upon conditions. While the corrosion pits only nucleate under fairly extreme circumstances, they can continue to grow even when conditions return to normal since the interior of a pit is naturally deprived of oxygen and locally the pH decreases to very low values and the corrosion rate

increases due to an autocatalytic process. In extreme cases, the sharp tips of extremely long and narrow corrosion pits can cause stress concentration to the point that otherwise can shatter tough alloys; a thin film pierced by an invisibly small hole can hide a thumb sized pit from view. These problems are especially dangerous because they are difficult to detect before a part or structure fails. Pitting remains among the most common and damaging forms of corrosion in passivated alloys but it can be prevented by control of the alloy's environment [Frankel (1998)].

Pitting results when a small hole, or cavity, forms in the metal usually as a result of de-passivation of a small area. This area becomes anodic, while part of the remaining metal becomes cathodic producing a localized galvanic reaction. The deterioration of this small area penetrates the metal and can lead to failure. This form of corrosion is often difficult to detect due to the fact that it is usually relatively small and may be covered and hidden by corrosion-produced compounds.

3. Crevice Corrosion

Crevice corrosion is a localized form of corrosion occurring in confined spaces (crevices), to which the access of the working fluid from the environment is limited. Formation of a differential aeration cell leads to corrosion inside the crevices. Examples of crevices are gaps and contact areas between parts under gaskets or seals, inside cracks and seams, spaces filled with deposits and under sludge piles [Hu et al. (2011)].

Crevice corrosion is influenced by the crevice type (metal-metal, metal-nonmetal), crevice geometry (size, surface finish), and metallurgical and environmental factors. The susceptibility to crevice corrosion can be evaluated with ASTM standard procedures. A critical crevice corrosion temperature is commonly used to rank a material's resistance to crevice corrosion.

4) Microbial Corrosion

Microbial corrosion, or commonly known as microbiologically influenced corrosion (MIC) is a corrosion caused or promoted by micro organisms usually chemoautotrophs. It can apply to both metallic and non-metallic materials in the presence or absence of oxygen. Sulfate-reducing bacteria are active in the absence of oxygen (anaerobic); they produce hydrogen sulfide, causing sulfide stress cracking. In the presence of oxygen (aerobic) some bacteria may directly oxidize iron to iron oxides and hydroxides, other bacteria oxidize sulfur and produce sulfuric acid causing biogenic sulfide corrosion. Concentration cells can form in the deposits of corrosion products leading to localized corrosion [Zarasvand and Rai (2010)].

Accelerated low-water corrosion (ALWC) is a particularly aggressive form of MIC that affects steel piles in seawater near the low water tide mark. It is characterized by an orange sludge which smells of hydrogen sulfide when treated with acid. Corrosion rates can be very high and design corrosion allowances can soon be exceeded leading to premature failure of the steel pile. Piles that have been coated and have cathodic protection installed at the time of construction are not susceptible to ALWC. For unprotected piles sacrificial anodes can be installed local to the affected areas to inhibit the corrosion or a complete retrofitted sacrificial anode system can be installed. Affected areas can also be treated electrochemically by using an electrode to first produce chlorine to kill the bacteria and then to produce a calcareous deposit which will help shield the metal from further attack.

5) High Temperature Corrosion

High-temperature corrosion is chemical deterioration of a material (typically a metal) as a result of heating. This non-galvanic form of corrosion can occur when a metal is subjected to a hot atmosphere containing oxygen, sulfur or other compounds capable of oxidizing (or assisting the oxidation of) the material concerned. For example, materials used in aerospace, power generation and even in car engines have to resist

sustained periods at high temperature in which they may be exposed to an atmosphere containing potentially highly corrosive products of combustion [Oksa et al. (2014)].

The products of high-temperature corrosion can potentially be turned to the advantage of the engineer. The formation of oxides on stainless steels, for example, can provide a protective layer preventing further atmospheric attack, allowing for a material to be used for sustained periods at both room and high temperatures in hostile conditions. Such high-temperature corrosion products, in the form of compacted oxide layer glazes, prevent or reduce wear during high-temperature sliding contact of metallic (or metallic and ceramic) surfaces [Lopez et al. (2014)].

Corrosion Measurement

Experimentally, one measures polarization characteristics by plotting the current response as a function of the applied potential. Since the measured current can vary over several orders of magnitude, usually the log current function is plotted vs. potential on a semi-log chart. This plot is termed a potentiodynamic polarization plot. It is to be noted that the use of a semi-log display prevents indication of polarity on such plots. Potentials negative of E_{corr} give rise to cathodic currents, while potentials positive of E_{corr} give rise to anodic currents.

Fig. 4.2 shows the potentiodynamic anodic polarization plot of a sample of 430 stainless steel. The logarithm of the current is plotted (the abscissa) as a function of the applied potential (the ordinate). Region A in Figure 4.2is the active region, in which the metal specimen corrodes as the applied potential is made more positive. At B, further increase in the rate of corrosion (as measured by the current) ceases and the onset of passivation begins. The loss of chemical reactivity under certain environmental conditions, probably due to the formation of a film on the surface of the metal is referred to as specimen passivation. This point is characterized by two coordinate values, the primary passive potential (EPP) and the critical current density (I_c). In region C, the current decreases rapidly as the passivating film forms on the specimen. A small secondary peak is observed followed by region D, where there is

little change in current as the potential is increased. The passivating film begins to break down in region E, the transpassive region.

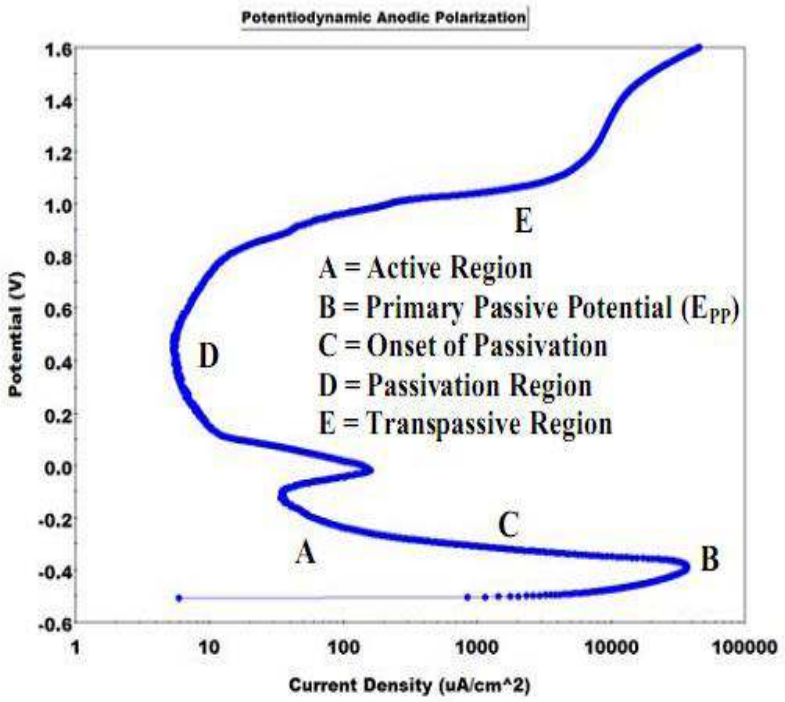

Fig. 4.2 Standard potentiodynamic anodic polarization plot of 430 stainless steel
[Princeton Applied Research]

A potentiodynamic anodic polarization plot such as Fig. 4.2 can yield important information such as:

1. The ability of the material to spontaneously passivate in the particular medium.

2. The potential region over which the specimen remains passive.

3. The corrosion rate in the passive region.

The following discussion will deal with a class of metals or nanocomposites that can exhibit active to passive behavior. Whether a specimen will or will not passivate depends on the form and intersection of the individual anodic and cathodic polarization plots.

Tafel Plots

Electrochemical techniques of corrosion measurement are currently experiencing increasing popularity among corrosion engineers due primarily to the rapidity with which these measurements can be made. Long term corrosion studies such as weight loss determinations, may take days or weeks to complete while an electrochemical experiment will require, at most, several hours. The speed of electrochemical measurements is especially useful for those metals or alloys that are highly corrosion resistant.

A Tafel plot is performed on a metal or metal based nanocomposite specimen by polarizing the specimen about 300 mV anodically (positive-going potential) and cathodically (negative-going potential) from the corrosion potential, E_{corr}, as shown in Fig. 4.3. The potential does not have to be scanned but can be "stepped" in a staircase waveform if desired. The resulting current is plotted on a logarithmic scale as shown in Figure 4.4.

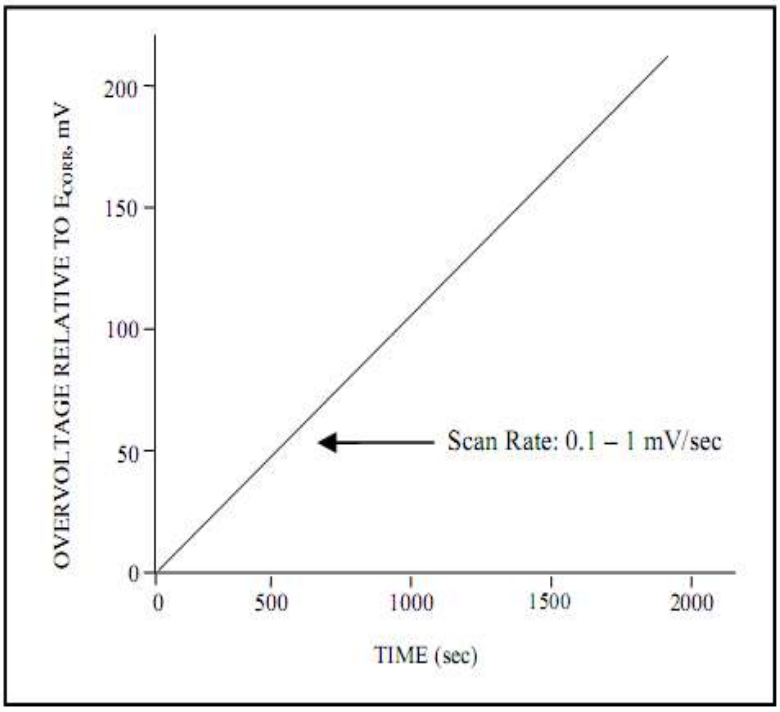

Fig. 4.3 Excitation waveform for Tafel plots
[Princeton Applied Research]

The anodic or cathodic Tafel plots are described by the Tafel equation:

$$\eta = \beta \log \frac{I}{I_{corr}} \qquad (4.14)$$

Where, η = overvoltage is the difference between the potential of the specimen and the corrosion potential.

β = Tafel constant

I_{corr} = current at overvoltage η, μA.

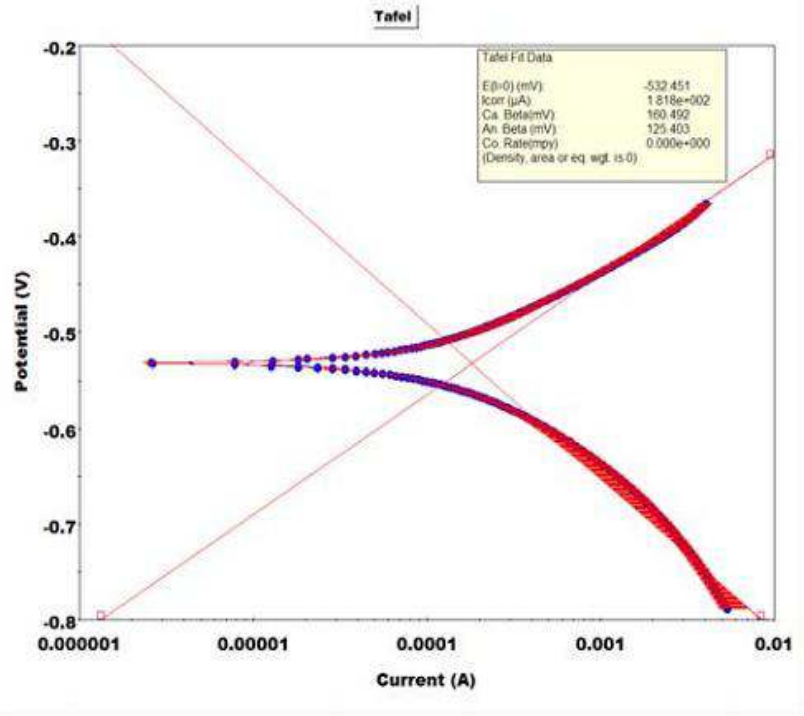

Fig. 4.4 Experimentally measured Tafel plot
[Princeton Applied Research]

Formulae Used in Corrosion Measurements

$$C.R.(mpy) = \frac{0.13 I_{corr} (E.W.)}{d} \qquad (4.15)$$

Where, mpy= milli-inches per year.

I_{corr}= corrosion current density (μAcm^2)

E.W=equivalent weight of the corroding species, (g).

d= density of the corroding species, (g/cm^3).

$$\mu_p\,\% = (I^o_{corr} - I^i_{corr}) / I^o_{corr} * 100 \qquad (4.16)$$

Where, I^o_{corr} = values of corrosion current density in absence of reinforcement particles.

I^i_{corr} = values of corrosion current density in presence of reinforcement particles.

μ_p= Corrosion Protection Efficiency.

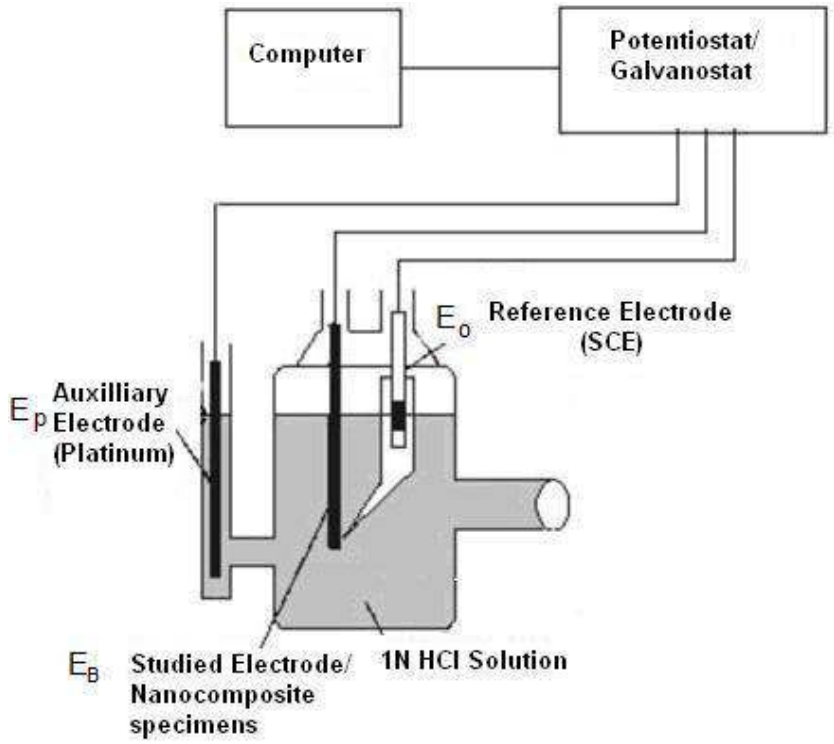

Fig. 4.5 Schematic Diagram showing the Corrosion Cell

Corrosion behavior of the specimens in the present case was studied using Gamry electrochemical cell having three electrodes connected to Gamry Instrument Potentiostat / Galvanostat with a Gamry framework system based on ESA400. Nanocomposite specimens were polished with emery polishing paper 600 no. and then with 12 μm diamond paste on a double disc polishing machine to remove any sort of stray marks from the surface of the specimen and to make it mirror polished. Gamry applications include software DC 105 for corrosion. Iron specimens with an exposed area of 1 cm^2 were used as working electrodes, platinum electrode was used as an auxiliary electrode and standard calomel electrode (SCE) was used as a reference electrode. All potentials were measured relative to SCE. Fig. 4.5 illustrates schematic diagram of corrosion cell. Tafel curves were obtained by changing the electrode potential automatically from -250 to + 250 mV versus corrosion potential (E_{corr}) at a scan rate of 1mV s^{-1}.

The present chapter elaborated the various characterization techniques in detail. Different characterization techniques discussed include X-ray diffraction, scanning electron microscopy, density, hardness, wear, deformation and corrosion respectively.

Chapter 5 to 9 describes the preparation and characterization of Fe-Al_2O_3 metal matrix nanocomposites, CoO and CeO_2 doped Fe-Al_2O_3 metal matrix nanocomposites and Fe-Al_2O_3-ZrO_2 hybrid metal matrix nanocomposites synthesized by powder metallurgy technique. The various properties investigated for the synthesized nanocomposite included phase, microstructure, density, hardness, wear, deformation and corrosion respectively.